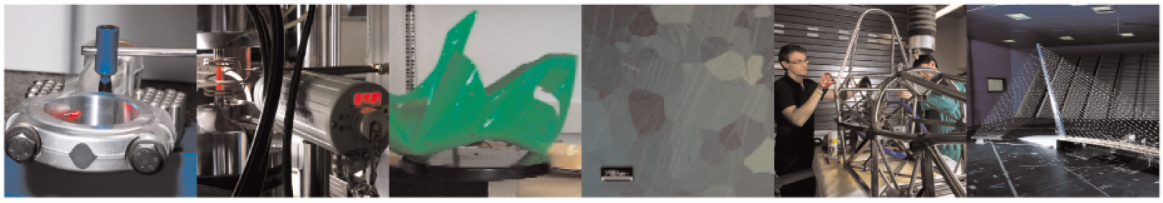
POLITECNICO
MILANO 1863

DIPARTIMENTO DI MECCANICA



An Experimental Investigation on Uncertainty in Measuring Vibration Deflection Shapes with Digital Image Correlation

Lavatelli A.;Balcaen R.;Zappa E.;Debruyne D.

This is a post-peer-review, pre-copyedit version of A. Lavatelli, R. Balcaen, E. Zappa and D. Debruyne, "An Experimental Investigation on Uncertainty in Measuring Vibration Deflection Shapes With Digital Image Correlation," in IEEE Transactions on Instrumentation and Measurement, vol. 69, no. 6, pp. 2826-2836, June 2020, doi: 10.1109/TIM.2019.2929876.

© 2019 IEEE. Personal use of this material is permitted. Permission from IEEE must be obtained for all other uses, in any current or future media, including reprinting/republishing this material for advertising or promotional purposes, creating new collective works, for resale or redistribution to servers or lists, or reuse of any copyrighted component of this work in other works.

This content is provided under CC BY-NC-ND 4.0 license

DIPARTIMENTO DI MECCANICA ■ POLITECNICO DI MILANO
via G. La Masa, 1 ■ 20156 Milano ■ EMAIL (PEC): pecmecc@cert.polimi.it
http://www.mecc.polimi.it
Rev. 0

An Experimental Investigation on Uncertainty in Measuring Vibration Deflection Shapes with Digital Image Correlation

Alberto Lavatelli, *Member, IEEE*, Ruben Balcaen, Emanuele Zappa, *Member, IEEE*, and Dimitri Debruyne

***Abstract*—3D Digital Image Correlation (DIC) is a widespread full field displacement measurement technique based on stereo vision. It was formulated to deal with static problems in experimental mechanics in the early seventies and since then the applicability of the technique increased due to increasing framerates and dropping prices of machine vision cameras. As a consequence DIC became a feasible solution for general purpose vibration testing. The present literature however does not offer a comprehensive analysis of DIC accuracy when applied to vibration testing and therefore this paper offers a "Type A" evaluation of uncertainty when measuring vibration deflection shapes with DIC. Uncertainty is evaluated for different experimental conditions on a stepped sine test. Data show that the average value of uncertainty normally lies below 0.02 mm but in resonant conditions it can increase up to 0.05 mm (considering a field of view of about half a meter). This demonstrates a strong correlation between the deflection amplitude and the random uncertainty due to motion blur.**

***Index Terms*—Digital Image Correlation, stereo DIC, uncertainty quantification, vibration testing**

I. Introduction

In recent years, Digital Image Correlation (DIC) has been proposed as a means to measure vibrations in applied experimental mechanics [1]. In the context of vibration testing DIC is interesting as it provides a contact-less measurement of full field oscillations [2], [3]. This feature is very interesting since the oscillation can be measured without load effects and without worrying about the sensor grid positioning. DIC can be compared to 3D-point tracking (3DPT) for what concerns displacement measurement. The two techniques have similar, if not identical, levels of uncertainty (roughly in the order of tenths of a pixel in operating conditions). However, DIC allows measurements of up to hundred thousand points from a surface, while 3DPT allows usually less than a hundred [1]. However, an analysis of literature shows that the application of DIC for vibration measurements may lead to a bias in the estimation of modal parameters [4], while at the same time the measurement uncertainty is somehow larger than what could be expected from the analysis of the measurement setup [5]–[7].

Manuscript received Xxxxx XX, 2018; revised Xxxxx XX, 2018.

A. Lavatelli is with the Department of Mechanical Engineering, Politecnico di Milano, Milan 20133, Italy (e-mail: alberto.lavatelli@polimi.it).

R. Balcaen is with the Materials Engineering department, KU Leuven, Gent 9000, Belgium (e-mail: ruben.balcaen@kuleuven.be).

E. Zappa is with the Department of Mechanical Engineering, Politecnico di Milano, Milan 20133, Italy (e-mail: emanuele.zappa@polimi.it).

D. Debruyne is with the Materials Engineering department, KU Leuven, Gent 9000, Belgium (e-mail: dimitri.debruyne@kuleuven.be).

In this work, the authors propose an experimental analysis of how the measurement uncertainty behaves during DIC based vibration testing, with focus on the estimation of deflection shapes. After a review of the state of the art of measurement uncertainty in photogrammetric vibration testing, the article proposes a methodology to evaluate the measurement accuracy of a deflection shape. The method is based on point cloud fitting and thus generically applicable. This is followed by an analysis of a stepped sine experiment which characterizes the uncertainty behavior with changing frequency, speckle patterns and excitation levels. A discussion of the results demonstrates how vibration signals from DIC are affected by noise whose level is correlated with the level of the signal. Moreover, noise analysis shows that after a certain amplitude threshold the Signal to Noise Ratio (SNR) drops noticeably.

As an element of novelty, this research demonstrates that uncertainty in DIC vibration monitoring is not constant with frequency and amplitude, but it is, conversely, a function of the two. This paper also shows how uncertainty depends on the dynamic stiffness of the test object as well as on the type of speckle pattern. Thus, it provides useful indications to design (or optimize) dynamic DIC experiments. These new elements may be applied to improve the reliability of DIC when used in the industrial field to perform design model validation [8], quality checks and structural health monitoring [1].

II. State of the art

Modal testing is a field of experimental mechanics dedicated to the experimental evaluation of the vibratory behavior of mechanical systems [9]. The output of this experimental method may include the determination of natural frequencies, damping factor, mode shapes and mode participation factors [10].

The use of DIC as a source for modal testing dates back to the early 2010s when Avitabile, Niezerecki et al. proposed the method as a source of full field vibration data for modal testing and structural dynamics [11], [12]. Also Helfrick et al., in the same period, experimented with DIC for vibration measurements [8]. Already in these first works it is possible to detect the strength and limitations of the DIC technique. Only after these first attempts, domain experts started to question the accuracy and the reliability of DIC based vibration measurements, which was to be expected since (stereo) DIC is a complex process of experimental, optical and programmatical components. While experimental

and optical error sources are theoretically well known in advance it can be hard to remove them in practice since one is usually limited by camera hardware (e.g. reduced pixel count leading to aliasing, uncorrected lens distortions [13], camera noise [14], reduced contrast [15], etc), speckle pattern characteristics [16] and uncontrollable environmental factors (e.g. air turbulence, image blur due to unwanted specimen motion, etc.). On the other hand there is the problem that DIC systems are usually a "black box" system in which various algorithmic parameters are shielded from the user. This while it is a must to tweak certain parameters depending on the application and set up. Some interpolants for example yield a lower bias in aliased conditions [17], while higher order shape functions should be chosen for cross-matching images when a high stereo angle is combined with a large subset size [18]. Despite these shortcomings DIC can yield decent results with an accuracy definitely below 0.1 pixels in regular conditions, thus being an interesting technique for full-field measurements. For our specific setup (see section III-A) this would result into a micrometer-scale accuracy. Warren et. al [19] performed a well designed experiment, validating 3D DIC (and 3D point tracking too), where photogrammetry is compared with two reference measurement methods: lasers vibrometers and accelerometers. Their activity was run on a fully controlled laboratory experiment. In the result it is possible to see that the estimation of the Frequency Response Function (FRF) with DIC data is different from the one performed with accelerometer data. This resulted in a bias between the two estimations of the modal parameters. However, due to the controlled experimental conditions, biases were below 2% for the estimation of natural frequencies. The accordance of mode shapes were always higher than 95%, while no data were given about the accuracy in estimating damping factors. In [20] it is showed that DIC proves to be less accurate and very noisy when the velocity of the specimen is very high, hence the suggestion that its applicability cannot be extended to generic vibration testing (thus substituting accelerometers). The same conclusions were stated also by [21].

All the previous analysis were performed in a controlled lab environment, in which all experimental conditions (including lighting of the scene) could be regulated arbitrarily. After these first lab attempts DIC moved to monitoring vibrations in operating conditions, especially on civil and large structures [7], [22]. In those contexts photogrammetric methods showed a higher uncertainty than expected and a loss in reliability was noticed. In [23], [24] the authors suggested that this additional uncertainty may be due to motion blur (caused by the finite exposure time of cameras and high velocity of the specimen). A further study [25] demonstrated that motion blur actively biases FRF estimation by underestimating the motion amplitude. This kind of bias is similar to the one created by choosing a poor windowing for the signal.

Our study, instead, focuses on the topic of assessing the uncertainty of shape reconstruction in dynamic applications. The aim is to evaluate how accurate the measurement of a dynamic shape deflection can be, while furthermore addressing the relationship with changing excitation frequencies, speckle pattern geometries and excitation levels.

III. Description of the Experiment

A. Experimental setup

The vision based vibration testing setup used in this paper is composed of 4 elements: a vibration shaker system, a stereo vision rig, an acquisition/control computer and a vibrating lamina. The relationship between the elements of the experimental setup is described in Figure 1.

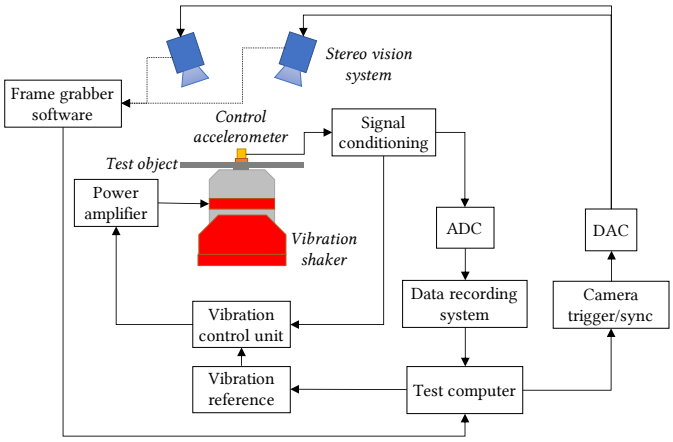


Figure 1. Functional scheme of the experimental setup

The vibration shaker system is composed of a *Data Physics* GW-V55 electromagnetic shaker and its GW-PA300E power amplifier (rated for 300 W rms power output). The system operates in the 2 Hz-8 kHz frequency band with a rated peak force of 311 N, with one inch of total travel and a maximum peak-to-peak velocity of $1.1\,\mathrm{m\,s^{-1}}$.

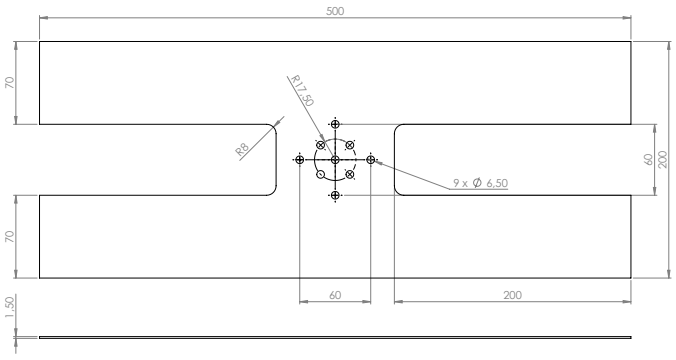
The stereo vision rig is composed by two FLIR Blackfly S BFS-U3-13Y3M-C cameras equipped with lenses having a nominal fixed focal length of 13 mm. The CMOS monochrome sensor dimension is 1280X1024 (1.3 Mpx), pixel size is $4.8\,\mu\mathrm{m}$ and its noise level is 2% of the dynamic range in operating conditions. The maximum acquisition frame rate for a single camera is 170 fps. The spatial resolution of the camera is evaluated according to the ISO 12233 standard 0,10SFR response level, which yields a sampling efficiency (E_S) of 93%.

The acquisition/control system is composed of a HP portable workstation and a National Instrument® (NI) modular instrumentation system. The instrumentation system is composed of two modules: a NI 9234 24-bit ± 5 V delta sigma DAC (with IEPE interface) to acquire the signal from the control accelerometer and a NI 9263 16-bit ± 10 V analog output module. The instrumentation is attached to the USB 2.0 hub of the computer and it is controlled by an in-house developed NI LabView® program which generates a pure sine wave. The shakers' amplitude is thus controlled with a closed-loop PID that feedbacks the signal of the control accelerometer to assure that the shaking table oscillates with the desired acceleration. The image acquisition is also managed by a LabView program, which synchronizes the acquisition of the two cameras by generating a TTL trigger signal which is sent to both cameras. The software pre-allocates RAM memory to store the images. Then the IMAQdx Labview library manages

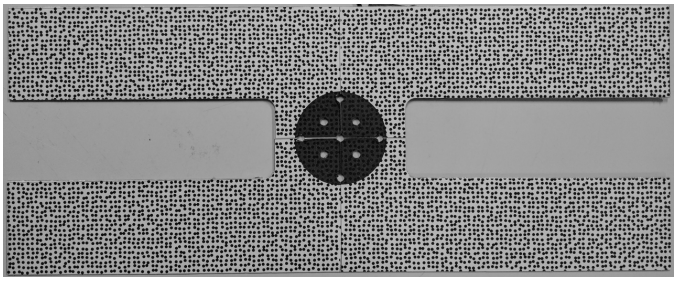
the USB 3.0 bus to grab the frames and store them in the hard drive when image acquisition is finished.

The stereo images are then DIC processed with the commercially available MatchID [26] software. DIC performs both stereo matching for the stereo pairs as well as time matching between each left and right frame. Given that the reference position of the test object is fixed, the DIC processing parameters (especially the area of interest, subset size and step) can be fixed too. As a flowchart, after each acquisition, the left and right images are saved in a folder, then MatchID is called from command line, thanks to its batch scripting interface. For each stereo pair the field of displacement (with respect to the reference position) is then computed thanks to space-temporal matching.

To test behavior of uncertainty, a suitable test rig has been designed. The first design constraint is imposed by limiting the operating frequency of the camera system. To avoid overloading the bandwidth of the USB 3.0 bus, the camera framerate was set to 100 fps, thus limiting the usable vibration frequency range to the 10-30 Hz band since aliasing has to be avoided. Consequently the testing system should be designed to have one or more resonances in the same frequency band. At the same time the system must be both lightweight and flexible to ensure that a wide range of deflection can be achieved with a simple shaker control system.



(a) Mechanical drawing



(b) Mechanical part with DIC pattern

Figure 2. H shape specimen

All the previous constraints are fulfilled by the design shown in Figure 2. The specimen is an H-shaped aluminum sheet ($1.5\,\mathrm{mm}$ thickness), whose shape nests 4 cantilever beams. The length of the beam is selected to have the first resonance frequency at about $20\,\mathrm{Hz}$ and the width is selected to allow enough subsets for DIC processing (so that the number of subsets in the transverse direction are 30% of the beam axis direction). The symmetrical structure allows the creation of closely spaced modes around the resonant frequency of a single beam leg.



Figure 3. Final mechanical test stand: the stereo camera are in the foreground, while shaker, specimen and lighting system lie in the background

The final setup is shown in Figure 3. The cameras are placed about $1\,\mathrm{m}$ away from the H-shape specimen to fill the field of view of the camera. It is important to highlight that the shaker system is insulated by a concrete basement suspended by a set of rubber pneumatic insulators. This ensures that no vibration is transmitted from the shaker to the camera system. The specimen was equipped with a strain gauge flexural half bridge to monitor vibrations and in order to have a quantitative idea of the natural frequencies of the final system. After a random excitation test, it was possible to locate 4 autospectrum peaks at $19.8\,\mathrm{Hz}$, $20.8\,\mathrm{Hz}$, $22.3\,\mathrm{Hz}$ and $22.7\,\mathrm{Hz}$. This accords with FEM analysis that predicts the existence of 4 closely spaced modes. The random test also shows that the first two peaks are highly damped with respect to the third and fourth peaks.

B. Design of the experiment

The goal of the experiment is to investigate the behavior of the deflection shape measurement uncertainty when the speckle pattern filling factor χ_P and excitation frequency changes, both at a constant excitation amplitude. So a single experiment is performed by doing a stepped sine test for each pattern spacing, for all the frequencies listed in Table I. Stepped sine testing is the easiest deflection shape measurement method and it is the best known to vibration test engineers. To recall the procedure, the frequency band under investigation is divided into discrete intervals. For each frequency of interest, the shaker is run with a pure sine excitation, which is closed loop controlled through software. The software is in-house developed with the LabView platform and provides PID control of excitation. The shaking table is equipped with a calibrated accelerometer, so that the feedback signal is the acceleration of the shaker.

The stepped sine is performed at a constant acceleration amplitude for all the frequencies of interest. When the shaker

frequency is changed, the mechanical system needs to achieve a steady regime before the data acquisition (the camera system in this case) is triggered and the test is recorded for the selected amount of time.

The speckle patterns are regular spaced speckle patterns: the dots have a fixed diameter d_p of $2.25\,\mathrm{mm}$ and the average in-centre spacing d_u is changed to achieve a more filled or, on the other hand, more sparse pattern. The speckle density factor χ_P here is defined as the ratio between d_p and d_u.

Table I
INVESTIGATION PATHS USED TO EXPERIMENTALLY ASSESS THE UNCERTAINTY IN DIC BASED VIBRATION TESTING

f [Hz]	
10	21.5
15	22
17	22.25
19	22.5
19.5	22.7
19.9	23
20	23.5
20.5	24
20.85	25
21	30

(a) Frequency path

Pattern code	d_u [mm]	χ_P [-]
A	2.42	0.93
B	2.77	0.81
C	3.12	0.72
D	3.46	0.65
E	3.81	0.59
F	4.15	0.54
G	4.5	0.50
H	4.85	0.46

(b) Pattern spacing path

The experiment is then performed at two different levels of excitation: $0.75\,\mathrm{m\,s^{-2}}$ and $1.50\,\mathrm{m\,s^{-2}}$. The outcome of the experimental activity is improved in this way since more data is obtained due to the doubling of the experiment, resulting in more statistical evidence built in, while on the other hand a better insight is given on the role of motion blur. More in detail, doubling the force is expected to increase the average speed of the specimen during vibration. This is expected to boost the level of motion blur, hence the uncertainty is expected to increase. The motion blur is generated by the convolution of target motion with the exposure time window. The acquisition parameters are: 100 frames per second with an exposure time of $2\,\mathrm{ms}$.

IV. SHAPE MEASUREMENT UNCERTAINTY BY FIT

If we consider a single snap of DIC images, the returned output is a 3D displacement map, with data points at the center of each subset (representing the continuous surface). The problem of determining the measurement uncertainty of a continuously deforming surface is however not trivial [27]. A first possible option is to compare DIC data with measurements coming from another full field surface displacement measurement system, such as Scanning Laser Doppler Vibrometers (SLDV). This is however very complex since a comparison of two measurement systems would require a uniform reference frame (for perfect alignment of data) and with similar useful frequency bands (which is hardly possible in the case of SLDV).

However, the authors suggest in previous works [23], [24] that in case of 3D DIC dynamic measurements, the random error is the most relevant contribution to uncertainty. That statement can be exploited to develop statistical tools able to estimate uncertainty straight from the DIC data, without having further comparisons with other measurement means. This way to proceed is in any case coherent with the "Type A" evaluation of random uncertainty, in conformity with ISO-GUM [28].

Analytically we can derive the uncertainty using a frequentist approach. The measured shape for the i-th image can be written as:

$$w_i(x,y) = w_0 + \varepsilon_w + w'_{(i)} \tag{1}$$

Where w_0 represents the actual shape of a surface Ω, ε_w the measurement bias, and w' is a random fluctuation of standard deviation σ_N. In this case, if we average all shape measurements we get:

$$\langle w \rangle = \lim_{n\to\infty} \frac{1}{n} \sum_{i=1}^{n} \left(w_0 + \varepsilon_w + w'_{(i)} \right) = w_0 + \varepsilon_w \tag{2}$$

With negligible bias the generic i-th frame becomes:

$$w_i(x,y) = w_0 + w'_{(i)} \tag{3}$$

Now, let us consider a scatter fit model $\Xi(x, y, \alpha_0, \cdots, \alpha_k)$ which supports fitting of continuous surfaces and is defined upon a set of α_k parameters. The fit model solves the problem in a least square sense, so that:

$$\left\{ \begin{array}{c} \alpha_0 \\ \vdots \\ \alpha_k \end{array} \right\} = \mathrm{argmin} \left[\iint_\Omega (\Xi - w_i)^2 \, dS \right] \tag{4}$$

Where dS represents the surface infinitesimal. Let us analyze the integral of quadratic error:

$$\begin{aligned} &\iint_\Omega (\Xi - w_i)^2 \, dS = \iint_\Omega \left(\Xi - w_0 - w'_{(i)}\right)^2 dS = \\ &= \iint_\Omega \Xi^2 + w_0^2 + w'^2_{(i)} - 2(\Xi w_0 + \Xi w'_{(i)} - w_0 w'_{(i)}) \, dS \end{aligned} \tag{5}$$

Given that the noise has a zero mean and no correlation to the signal, the covariance terms of the previous equation are identical to 0:

$$\begin{aligned} &\iint_\Omega w'^2_{(i)} dS = S_0 \, {\sigma_N}^2 \\ &\iint_\Omega \left(\Xi w'_{(i)} - w_0 w'_{(i)} \right) dS = 0 \end{aligned} \tag{6}$$

Where S_0 represents the total area of the measured shape. As a consequence the parameters of the fit are only defined by the true shape underlying the 3D point cloud (because the value of σ_N is independent from changes in α_k):

$$\begin{aligned} \left\{ \begin{array}{c} \alpha_0 \\ \vdots \\ \alpha_k \end{array} \right\} &= \mathrm{argmin} \left[\iint_\Omega (\Xi - w_0)^2 \, dS \right] = \\ &= \mathrm{argmin} \left[\iint_\Omega \left(\Xi^2 + w_0^2 - 2\Xi w_0 \right) dS \right] \end{aligned} \tag{7}$$

This demonstrates that the discrepancy between the fitted surface Ξ and the true shape w_0 is only due to the ability of the fit function to reproduce the geometry. So if we write the discrepancy between the point cloud and the fit surface in the generic point:

$$\Delta_F(x,y) = \Xi(x,y) - w_i(x,y) = \varepsilon_F(x,y) + w'(x,y) \tag{8}$$

Where ε_F represents the fit bias at the generic point (x, y). This proves that the difference between the 3D point cloud and the surface fit is only caused by the fit bias and random DIC errors. If the fit model is able to reproduce the shape of the surface, then $\varepsilon_F \ll \sigma_N$, hence:

$$u_S = \sqrt{\frac{\iint_\Omega {\Delta_F}^2 dS}{S_0}} = \\ = \sqrt{\frac{1}{S_0}\iint_\Omega \left[\varepsilon_F(x,y) + w'(x,y)\right]^2 dS} \approx \\ \approx \sqrt{\frac{1}{S_0}\iint_\Omega w'(x,y)^2\, dS} \tag{9}$$

In this case u_S represents the random component of shape measurement uncertainty for the generic 3D point cloud originated from a continuous surface.

A. LOWESS-spline fit procedure

Different approaches are available to fit the 3D point cloud of DIC data. In this case we chose to use a Locally Weighted Scatterplot Smoothing method (LOWESS), coupled with a cubic spline for data extension.

The LOWESS algorithm theory has been presented by Cleveland in [29]. The goal of LOWESS is to smooth out a generic point cloud using a local regression approach. The detailed implementation can be found in [30] and dates back to 1979, hence it is a mature and tested data analysis tool. For the purpose of this article it is useful to highlight some feature of the LOWESS approach.

LOWESS first divides the point cloud in subsets, which is followed by a local fit in the subset with a linear or quadratic polynomial model. This is however done in a non-parametric fashion, so that no hypothesis is done on the statistical distribution of the residuals. Given the non-parametric formulation, to achieve smoothing, the least squares problem is solved by using a weighted approach. In the formulation of Cleveland, the weight q_i for the i-th data point is a tri-cube weigth function of the distance d_i between the data point and the local fit function:

$$q_i = \left(1 - |d_i|^3\right)^3 \tag{10}$$

Once the subset has been fitted, the value of the LOWESS smoothing function for the point is retrieved by evaluating the local fit polynomial at the central point of the subset domain. In LOWESS methods, the level of smoothing is controlled by the size of the subsets. As one can imagine, the bigger the size, the lower the oscillation of data [29].

Given the subset-based non-parametric formulation of LOWESS, the smoothing procedure does not return a continuous surface. To provide continuity to data, it is necessary to connect the points with a suitable interpolant. In the original version [29], [30] data extension is performed with a linear interpolation of LOWESS output. In modern implementations, such as the one we used, data are extended with a cubic spline, so that C^2 continuity can be achieved.

B. Testing the approach with residuals

As it is possible to see in Figure 4 (where the deflected shape of a leg of the specimen described in Fig. 2 is measured), the LOWESS approach is able to accurately fit the DIC data and highlight the dispersion of the displacement field measurement.

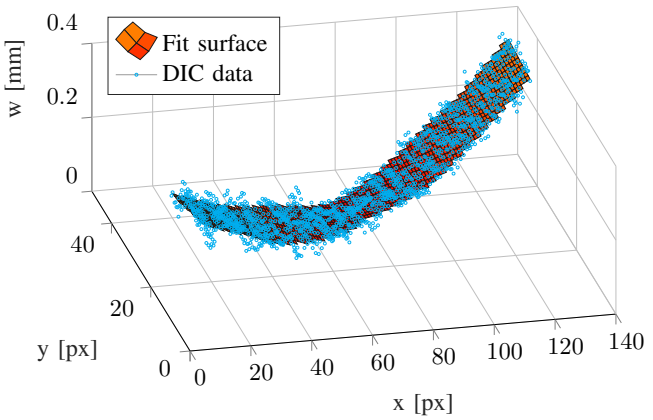


Figure 4. Fitting DIC datan from one leg of the H shape specimen of Fig. 2 with LOWESS smoothing. The dispersion of data can be highlighted visually

Thanks to the spline extension of data, it is always possible to evaluate the discrepancy $\Delta_F(x, y)$ between the surface fit and DIC data. If the discrepancy represents the random DIC error, then it is expected that the samples behave according to a zero-mean pseudo-normal distribution [31], [32]. As we can see in Figure 5, this happens with good significance over the entire measured surface. The Probability Density Function

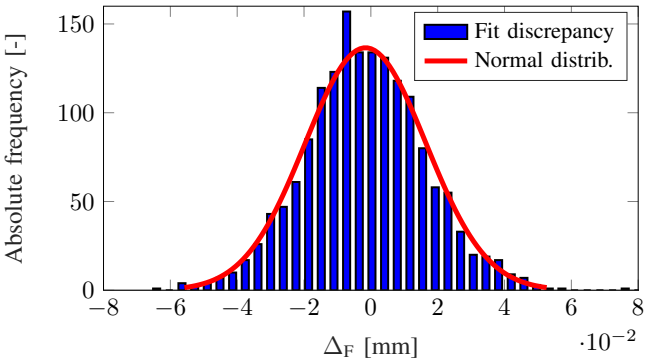


Figure 5. Distribution of fit discrepancy for DIC data of Figure 4

(PDF) of the random DIC error is known to be pseudo-normal due to the resolution limit and the non-linearity of the measurement chain. It should resemble a Gaussian distribution if the calibration is well performed, but usually the residuals do not pass the most popular normality tests. In Table II the results of Anderson-Darling [33], Shapiro-Wilk [34] and Lilliefor [35] tests are displayed. Shapiro-Wilk and Anderson-Darling are the most selective tests [36] and they both reject the hypothesis that the DIC random errors (as estimated by Δ_F) behave as a normal PDF. Lilliefors, instead, is less selective and fails to reject the null hypothesis. This proves that the fit residuals are pseudo-normal, but at the same time

Table II
RESULTS OF NORMALITY TESTS OF FIT DISCREPANCY OF FIGURE 4

	Anderson-Darling	Shapiro-Wilk	Lilliefor
Level of significance	5%	5%	5%
p-value	1.58%	0.02%	26.8%
Rejects null hypothesis	Yes	Yes	No

demonstrates the effectiveness of non-parametric smoothing provided by LOWESS. In fact LOWESS does not formulate a hypothesis on how the residuals are distributed. Therefore it is able to work correctly in this situation where the distribution of Δ_F clearly does not behave according to a simple theoretical normal PDF model.

V. EXPERIMENTAL UNCERTAINTY ANALYSIS

The goals of the experimental activity is to investigate the following topics related to DIC based vibration testing:

- How uncertainty changes with the frequency response of the structure.
- How uncertainty changes with a different speckle pattern density.
- Investigate what the SNR is for a given pattern during dynamic DIC tests.

This section discusses the uncertainty behavior for a single speckle pattern, as well as a comparative analysis of the performance of different speckle patterns. Finally an analysis of the SNR will demonstrate how DIC measurement uncertainty is deeply linked with the deflection amplitude.

A. Data processing method

The uncertainty estimation procedure is based on the approach described in Section IV. However this procedure estimates the uncertainty for a single set of (stereo) images. To extend the tool to steady state vibration, where i stereo pairs are acquired for each value of excitation frequency, some workaround is needed. In fact the uncertainty value is different frame by frame because both the deflection shape and the average instantaneous velocity (which is the main cause of motion blur) changes every time an image is registered. This leads to the need of a synthetic index to quantify the measurement uncertainty.

The first step is to fit every DIC point cloud $w_i(x,y)$ with the LOWESS model, so that each frame has its own $\Xi_{(i)}(x,y)$ interpolant. Consequently, the fit discrepancy $\Delta_F^{(i)}(x,y)$ and the uncertainty estimator $u_S^{(i)}$ (computed as in (11)) can be obtained for the generic i-th image pair. To have a metric which allows us to summarize the average deflection of the whole shape of the i-th image pair, we can introduce the deflection index a_S as the standard deviation of fitted shape $\Xi_{(i)}(x,y)$, defined as:

$$a_S^{(i)} = \sqrt{\frac{1}{S_0} \cdot \iint_\Omega \left(\Xi_{(i)} - \left\langle \Xi_{(i)} \right\rangle\right)^2 dS} \tag{11}$$

Now for each acquired image pair an estimator of the surface average value of uncertainty $u_S^{(i)}$ and another for deflection $a_S^{(i)}$ are available. This allows us to calculate the average uncertainty and deflection at the j-th frequency as:

$$\begin{cases} U_j = \left\langle u_S^{(i)} \right\rangle = \frac{1}{N} \sum_{i=1}^{N} u_S^{(i)} \\ A_j = \left\langle a_S^{(i)} \right\rangle = \frac{1}{N} \sum_{i=1}^{N} a_S^{(i)} \end{cases} \tag{12}$$

To conclude data processing, this operation is repeated for every j-th frequency of the stepped sine test, so it is possible to compute how the average surface deflection and uncertainty changes with varying frequencies. Therefore, the uncertainty characteristic of a pattern can be displayed as uncertainty as a function of frequency $U_j(f_j)$ or as uncertainty as a function of shape deflection $U_j(A_j)$.

B. Behavior of the single pattern during stepped sine test

The first result of this research activity is the characterization of the behavior of uncertainty when frequency changes. Since previous studies [23], [24] demonstrated the role of motion blur in DIC uncertainty, it is expected that the measurement uncertainty should increase significantly when the system is excited at one of its natural frequencies. If the vibration forcing remains constant during the frequency sweep, the deflection of the system greatly increases when passing an excitation period that is close to the one of a resonant frequency (as long as the system is under-damped).

Figure 6 indicates that the frequency behavior of the deflection shape uncertainty follows the expectations, as well as the expected behavior of the FRF of the mechanical system. In static conditions, the uncertainty is mainly ruled by noise and image processing biases. As the system approaches a resonant frequency, it starts to deflect more and more, until motion blur becomes the main source of uncertainty. It is interesting to see the relationship between the system deflection and the measurement uncertainty. Another feature highlighted in Figure 6 is that the uncertainty of DIC as a vibration measurement system is correlated with the vibration itself; the uncertainty rises with increasing deflection.

Synthetic experiments demonstrated in [24] that the measurement uncertainty of DIC in motion blurred conditions should follow a power law model as a function of the amount of motion blur. Motion blur itself is proportional to the instantaneous speed of the measurand during exposure time. Now, since the test is run with steady state vibrations, the amount of motion blur is proportional to velocity, which in its turn is proportional to the deflection amplitude. In this study, it is proposed to fit the uncertainty vs amplitude data with a power law model formulated as:

$$u_e = c_0 \left(1 + a^{c_1}\right) \tag{13}$$

As we can see in Figure 7, the power law model fits well the data. Beside the power law model behavior, it is important to highlight that there is evidence that the motion blur uncertainty is strongly correlated with the motion of the structure. In this situation the random uncertainty component of the signal (that

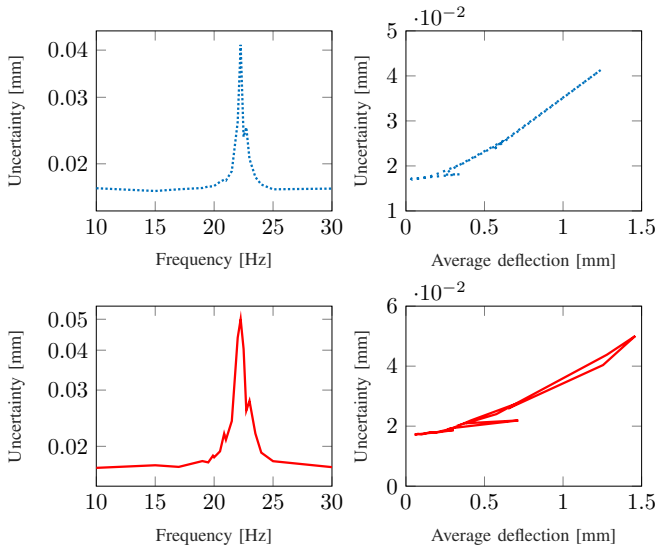


Figure 6. Frequency behavior of uncertainty for speckle pattern C (see Table I) applied to the specimen. Blue dotted data are about the 0.75 ms^{-2} test, while red solid are about the 1.50 ms^{-2} test.

we may address with the generic term of noise) is not anymore uncorrelated with the signal. A deeper analysis of this topic will be provided further in paragraph V-D.

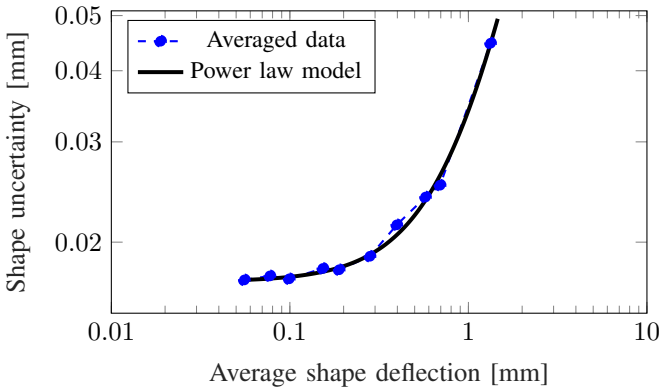


Figure 7. Uncertainty motion characteristics of pattern C when excitation level is 1.50 ms^{-2}

C. Comparing pattern performances

The experiment highlighted in the previous chapter was re-run for every pattern spacing of the designed experiment. The first output of the analysis are the uncertainty surfaces displayed in Figure 8. The diagram displays the uncertainty, plotted against in-centre spacing and excitation frequency. In this diagram it is possible to see that uncertainty is very sensitive to changes in the experimental conditions.

However with two separate diagrams for each forcing amplitude it is hard to understand the role of vibration forcing in the generation of uncertainty. A better summary of the behavior of mode shape uncertainty with changing experimental parameters can be found in Figure 9. The first row of the figure displays how uncertainty changes in different testing conditions: when the system is excited at frequencies lower than the resonant ones (10 to 17 Hz), when the system is excited around its natural frequencies (19.5 to 23 Hz) and when the system is excited at frequencies higher than the resonant ones (23.5 to 30 Hz). The diagrams are obtained by averaging the uncertainty values of each pattern for the three frequencies ranges specified above. The diagrams clearly demonstrate that, out of the resonance range, for both the levels of excitation, the uncertainty is minimized with very dense and filled patterns. The uncertainty is however minimized by more spaced speckled patterns in resonant conditions. It is also interesting to see that the uncertainty is more sensitive to the level of excitation as the dynamic stiffness decreases. At low frequencies there is not an evident difference between the uncertainty at lower and higher forcing. This suggests that in those conditions DIC measurements are performed in a quasi-static manner. In resonant conditions, instead, it is expected that the system deflects consistently. Hence the bigger the deflection, the higher the motion blur and consequently the higher the uncertainty. This expectation is verified by data, with the uncertainty at the higher level of excitation being about 60% bigger than at the lower level of excitation. After resonance, the dynamic stiffness of the structure is in this case lower than pre-resonance, so the offset between the two levels of forcing is more noticeable. The deflection is in any case much smaller after resonance, so that the difference in uncertainty is less relevant than in resonant conditions.

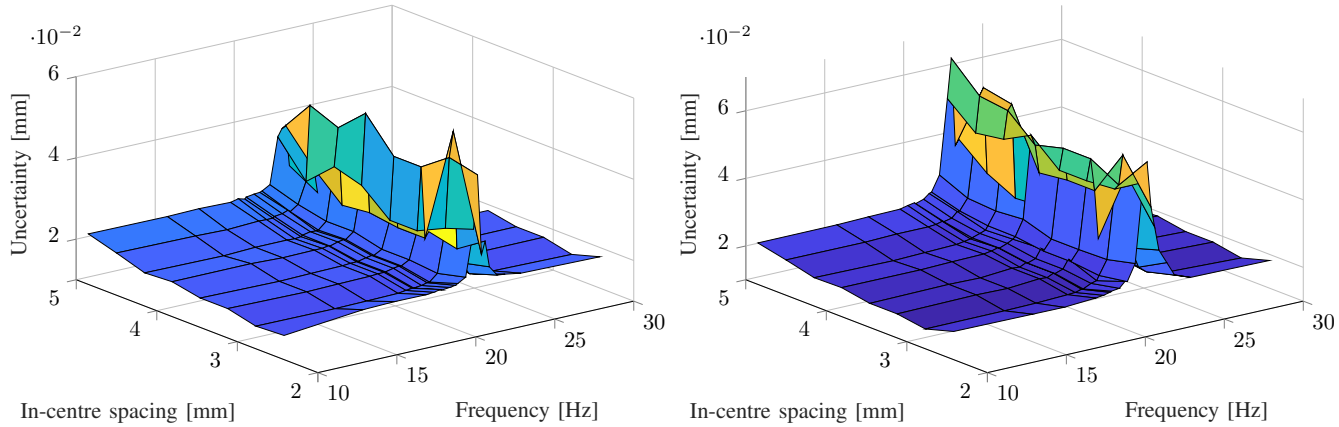
The graph in the second row of Figure 9 provides a more synthetic metric on how uncertainty changes with the frequency sweep. It is computed by averaging the uncertainty vs frequency data for all the tested patterns. So, no matter how the pattern is, there is a repeatable trend of uncertainty changing evidently as the frequency of excitation passes through the resonant frequencies of the system. In addition we can see that this "pseudo-spectrum" of uncertainty is amplified as the level of excitation is raised, which is justified by the presence of motion blur. When passing through resonances, the average value of shape deflection measurement uncertainty is in any case in the same order of magnitude. However the maximum value of uncertainty in resonant conditions can be 2 to 3 times higher than the ones pre- or post-resonance.

D. SNR analysis

In paragraph V-B it has been demonstrated how the measurement uncertainty is correlated with the signal. The uncertainty target in this work is a random fluctuation identical to a generic measurement noise. The correlation between uncertainty and signal is modeled as the power law of eq.(13). As a consequence the ratio between the amplitude of motion and the previously mentioned formula estimates the signal-to-noise ratio (SNR) for the i-th pattern:

$$SNR_{(i)} = \frac{a}{c_0^{(i)}\left(1 + a^{c_1^{(i)}}\right)} = \frac{1}{c_0^{(i)} a^{-1} + c_0^{(i)} a^{c_1^{(i)}-1}} \quad (14)$$

The fitting procedure highlighted in paragraph V-B has been repeated for each pattern, resulting in a characterization of the SNR as a function of the pattern spacing. The results are displayed in Table III. The first necessary comment is



(a) Amplitude 0.75 ms^{-2} (b) Amplitude 1.50 ms^{-2}

Figure 8. Uncertainty surfaces obtained for the experiment. Uncertainty is a function of frequency, pattern spacing and level of forcing.

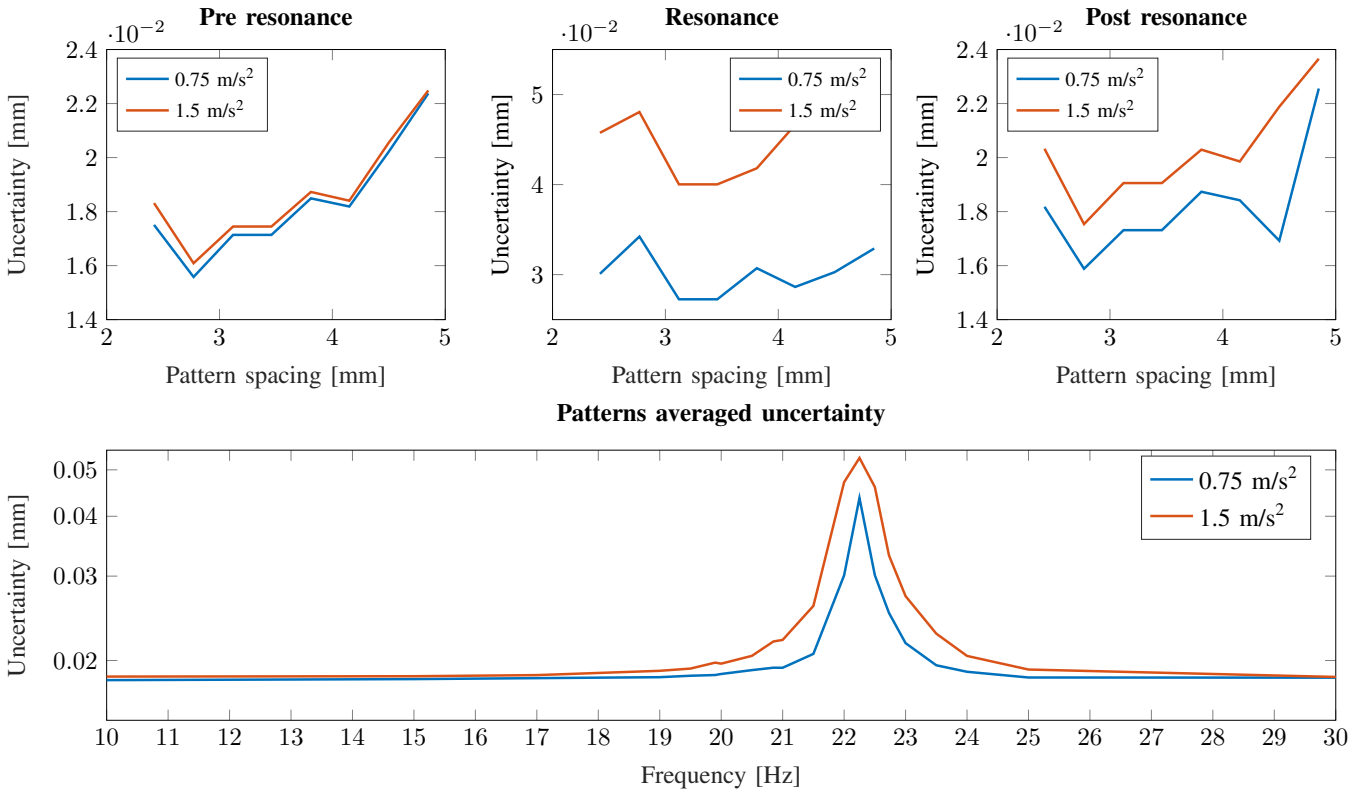


Figure 9. Comparative uncertainty analysis for the designed experiment. Uncertainty as a function of excitation frequency, pattern geometry and levels of excitation.

that coefficient c_1 is always larger than 1 for all patterns. By looking at the denominator of eq.(14), it is possible to see that the first term decreases asymptotically as the vibration amplitude increases. Conversely, the exponent of the second term is always larger than 0, hence it increases as the amplitude increases. In this way it is clear that the value of the SNR does not monotonically increases as for a sensor whose noise is uncorrelated with the measurand. Instead the SNR will display a maximum value, followed by a reduction as the vibration amplitude increases.

This behavior can be seen in Fig.10, where the SNR data

Table III
POWER LAW FIT PARAMETERS FOR EACH PATTERN AT 1.50 MS^{-2} EXCITATION

Pattern code	c_0 [mm]	c_1 [-]	a_C [mm]
A	0.0176	1.46	1.7063
B	0.0165	1.76	1.17
C	0.0170	1.70	1.24
D	0.0170	1.70	1.24
E	0.0172	1.24	3.18
F	0.0174	1.46	1.69
G	0.0199	1.76	1.17
H	0.0211	1.67	1.27

is plotted for each pattern type. In the region between 0.01 and 1 mm of average shape motion, the pattern behaves like an ideal uncorrelated noise sensor. Their SNR is very similar, hence DIC performs equally well. As the amplitude becomes bigger than a certain threshold, SNR drops fast, with each pattern following a different slope. The critical amplitude a_C where the SNR is inverted can be computed as in eq.(15) by finding the maximum point of eq.(14).

$$a_C = \left(\frac{1}{c_1 - 1}\right)^{\frac{1}{c_1}} \tag{15}$$

The list of critical amplitudes for the tested patterns can be found in Table III. It is possible to see that pattern E with (i.e. χ_P=0.59) outperforms the other patterns, since it provides the best compromise between static performance and resistance to motion blur.

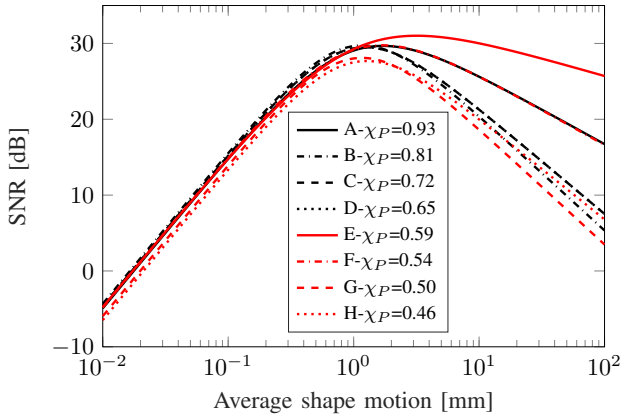


Figure 10. SNR characteristics of patterns for the stepped sine experiment at 1.50 ms^{-2} level of forcing

E. Discussion of results

The experimental investigation on the uncertainty of DIC based vibration testing has provided an interesting characterization of how measurement noise behaves in those testing conditions. The main findings can be summarized in this list:

- When using DIC to monitor vibration, random uncertainty (measurement noise in other words) is correlated with the motion of the system due to the action of motion blur.
- This correlation between signal and noise follows a power law behavior which is different from one speckle pattern to another.
- Given that, SNR is not a monotonically increasing variable, but as motion increases (so signal increases) there's a critical point over which the SNR drops rapidly.
- The lower the deflection of the specimen, the lower the motion blur on the image. As a consequence, the system performs well in "quasi-static" conditions (slight motion blur).
- Around resonances motion blur is higher and more sparse patterns can minimize the measurement uncertainty in those conditions.

The problem of noise being correlated with motion is a generically worrying feature in the use of DIC for vibration testing, since the generic modal identification algorithm (both for Experimental Modal Analysis and Operational Modal Analysis) models noise as a random process which is uncorrelated with the signals.

Moreover the frequency response functions are estimated by hypothesizing that the covariance of noise between each measurement signal is equal to zero. Both these two hypothesis are not true in the context of DIC vibration measurement. This means that, depending on the kind of problem, model identification may become harder or impossible with state of the art methods.

A final note to make a better context of this experiment is on the level of exposure. This experiment has been run with reasonable levels of exposure time, therefore the values of motion blur considered in the analysis are realistic. In fact, considering the frequency sweep displayed in Table I, the exposure ranges from 2% to 6% of the vibration period, which is a completely normal operating spectrum for a camera based vibration measurement. In fact the maximum values of motion blur during a period of oscillation are in the order of a couple of pixels for the lower level of excitation and in the order of 5 pixels for the higher one. The average values, instead, are much lower. This demonstrates that even slight levels of motion blur can play a relevant role in generating uncertainty.

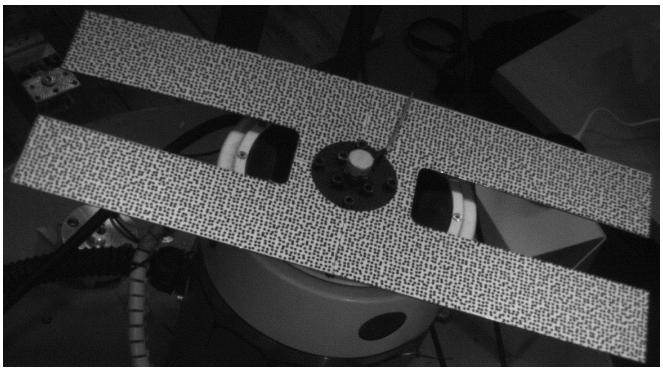


Figure 11. Highest level of motion blur for the 0.75 ms^{-2} level of forcing for pattern D. Speckle blurring is almost not detectable at naked eye.

VI. Conclusion

This paper proposes an experimental investigation of measurement uncertainty of stereo DIC applied to the measurement of vibration deflection shapes. This investigation performed a "Type A" evaluation of the random uncertainty component of DIC measurements. This component is the main uncertainty source when performing dynamic displacement measurements with DIC.

The analysis shows that the measurement uncertainty is not a constant value during a stepped sine vibration testing. Instead the uncertainty of shape measurements grows when passing through resonances. This phenomenon is due to motion blur and it correlates the level of noise with the amplitude of the shape deflection. The results analysis shows that every speckle pattern has a particular SNR signature and a different

limit of applicability (in terms of operative range of deflection amplitude at which the measurement can be carried on with good quality).

The correlation between noise and signal suggests that the outcome of state of the art modal identification algorithms may be biased or less reliable than what would be expected for accelerometer based vibration testing. Consequently future developments of this study will investigate this issue.

REFERENCES

[1] J. Baqersad, P. Poozesh, C. Niezrecki, and P. Avitabile, "Photogrammetry and optical methods in structural dynamics – a review," *Mech. Syst. Sig. Process.*, vol. 86, pp. 17 – 34, 2017. Full-field, non-contact vibration measurement methods: comparisons and applications.

[2] J. G. Gualtieri and J. A. Kosinski, "Large-area, real-time imaging system for surface acoustic wave devices," *IEEE Trans. Instrum. Meas.*, vol. 45, pp. 872–878, Oct 1996.

[3] X. Maurice, C. Doignon, and D. Knittel, "On-line vibrations characterization of a moving flexible web with a fast structured lighting stereovision system," in *2007 IEEE Instrumentation Measurement Technology Conference IMTC 2007*, pp. 1–5, May 2007.

[4] P. L. Reu, D. P. Rohe, and L. D. Jacobs, "Comparison of DIC and LDV for practical vibration and modal measurements," *Mech. Syst. Sig. Process.*, vol. 86, pp. 2 – 16, 2017.

[5] P. Poozesh, J. Baqersad, C. Niezrecki, and P. Avitabile, *Advancement of Optical Methods in Experimental Mechanics, Volume 3: Proceedings of the 2015 Annual Conference on Experimental and Applied Mechanics*, ch. A Multi-camera Stereo DIC System for Extracting Operating Mode Shapes of Large Scale Structures, pp. 225–238. Cham: Springer International Publishing, 2016.

[6] P. Poozesh, J. Baqersad, C. Niezrecki, E. Harvey, and R. Yarala, "Full-field inspection of a utility scale wind turbine blade using digital image correlation," in *CAMX 2014 - Composites and Advanced Materials Expo: Combined Strength. Unsurpassed Innovation*, 2014.

[7] P. Poozesh, J. Baqersad, C. Niezrecki, P. Avitabile, E. Harvey, and R. Yarala, "Large-area photogrammetry based testing of wind turbine blades," *Mech. Syst. Sig. Process.*, pp. –, 2016.

[8] M. N. Helfrick, C. Niezrecki, P. Avitabile, and T. Schmidt, "3d digital image correlation methods for full-field vibration measurement," *Mech. Syst. Sig. Process.*, vol. 25, no. 3, pp. 917 – 927, 2011.

[9] D. J. Ewins, *Modal Testing: Theory, Practice and Application*. Mechanical Engineering Research Studies: Engineering Dynamics Series, John Wiley & Sons, Limited, 2 ed., 2017.

[10] C. de Silva, *Vibration Monitoring, Testing, and Instrumentation*. Mechanical and Aerospace Engineering Series, CRC Press, 2007.

[11] P. Avitabile, C. Niezrecki, M. Helfrick, C. Warren, and P. Pingle, "Noncontact measurement techniques for model correlation," *Sound and Vibration*, vol. 44, no. 1, pp. 8–13, 2010.

[12] C. Niezrecki, P. Avitabile, C. Warren, P. Pingle, and M. Helfrick, "A review of digital image correlation applied to structural dynamics," vol. 1253, pp. 219–232, 2010.

[13] Z. Zhang, "A flexible new technique for camera calibration," *IEEE Trans. Pattern Anal. Mach. Intell.*, vol. 22, pp. 1330–1334, Nov 2000.

[14] Z. Gao, X. Xu, Y. Su, and Q. Zhang, "Experimental analysis of image noise and interpolation bias in digital image correlation," *Opt. Lasers Eng.*, vol. 81, pp. 46–53, 2016.

[15] P. Reu, "All about speckles: Contrast," *Exp. Tech.*, vol. 39, no. 1, pp. 1–2, 2015.

[16] P. Mazzoleni, E. Zappa, F. Matta, and M. Sutton, "Thermo-mechanical toner transfer for high-quality digital image correlation speckle patterns," *Opt. Lasers Eng.*, vol. 75, pp. 72–80, 2015.

[17] R. Balcaen, P. Reu, P. Lava, and D. Debruyne, "Stereo-DIC uncertainty quantification based on simulated images," *Exp. Mech.*, vol. 57, no. 6, pp. 939–951, 2016.

[18] H. Schreier and M. Sutton, "Systematic errors in digital image correlation due to undermatched subset shape functions," *Exp. Mech.*, vol. 42, no. 3, pp. 303–310, 2002.

[19] C. Warren, C. Niezrecki, P. Avitabile, and P. Pingle, "Comparison of frf measurements and mode shapes determined using optically image based, laser, and accelerometer measurements," *Mech. Syst. Sig. Process.*, vol. 25, no. 6, pp. 2191 – 2202, 2011.

[20] T. Beberniss, T. Eason, and S. Spottswood, "High-speed 3d digital image correlation measurement of long-duration random vibration; recent advancements and noted limitations," vol. 2, pp. 1403–1415, Katholieke Universiteit Leuven, 2012.

[21] D. Ehrhardt, S. Yang, T. Beberniss, and M. Allen, "Mode shape comparison using continuous-scan laser doppler vibrometry and high speed 3d digital image correlation," vol. 6, pp. 321–331, Springer New York LLC, 2014.

[22] G. Busca, A. Cigada, P. Mazzoleni, and E. Zappa, "Vibration monitoring of multiple bridge points by means of a unique vision-based measuring system," *Exp. Mech.*, vol. 54, no. 2, pp. 255–271, 2014.

[23] A. Lavatelli and E. Zappa, "Modeling uncertainty for a vision system applied to vibration measurements," *IEEE Trans. Instrum. Meas.*, vol. 65, pp. 1818–1826, Aug 2016.

[24] A. Lavatelli and E. Zappa, "A displacement uncertainty model for 2-d dic measurement under motion blur conditions," *IEEE Trans. Instrum. Meas.*, vol. 66, pp. 451–459, March 2017.

[25] A. Lavatelli and E. Zappa, "Uncertainty in vision based modal analysis: Probabilistic studies and experimental validation," *Acta IMEKO*, vol. 5, no. 4, pp. 37–48, 2016.

[26] MatchID, "http://www.matchidmbc.com/." Drongen, Belgium.

[27] R. Anchini, C. Liguori, V. Paciello, and A. Paolillo, "A comparison between stereo-vision techniques for the reconstruction of 3-d coordinates of objects," *IEEE Trans. Instrum. Meas.*, vol. 55, pp. 1459–1466, Oct 2006.

[28] ISO, "Guide 98-3:2008 - Guide to the expression of uncertainty in measurement (GUM:1995)," 2008.

[29] W. S. Cleveland, "Robust locally weighted regression and smoothing scatterplots," *J. Am. Stat. Assoc.*, vol. 74, no. 368, pp. 829–836, 1979.

[30] W. S. Cleveland, "Lowess: A program for smoothing scatterplots by robust locally weighted regression," *The American Statistician*, vol. 35, no. 1, pp. 54–54, 1981.

[31] Z. Wang, H. Li, J. Tong, and J. Ruan, "Statistical analysis of the effect of intensity pattern noise on the displacement measurement precision of digital image correlation using self-correlated images," *Exp. Mech.*, vol. 47, no. 5, pp. 707–707, 2007.

[32] M. Sutton, J. Orteu, and H. Schreier, *Image Correlation for Shape, Motion and Deformation Measurements: Basic Concepts,Theory and Applications*. Springer US, 2009.

[33] T. W. Anderson and D. A. Darling, "Asymptotic theory of certain "goodness of fit" criteria based on stochastic processes," pp. 193–212, 1952.

[34] S. S. Shapiro and M. B. Wilk, "An analysis of variance test for normality (complete samples)," *Biometrika*, vol. 52, no. 3-4, pp. 591–611, 1965.

[35] H. W. Lilliefors, "On the kolmogorov-smirnov test for normality with mean and variance unknown," *J. Am. Stat. Assoc.*, vol. 62, no. 318, pp. 399–402, 1967.

[36] N. M. Razali, Y. B. Wah, *et al.*, "Power comparisons of shapiro-wilk, kolmogorov-smirnov, lilliefors and anderson-darling tests," *Journal of statistical modeling and analytics*, vol. 2, no. 1, pp. 21–33, 2011.

Alberto Lavatelli - M'2014 received in 2015 the M.Sc. degree in Mechanical Engineering from the Polytechnic University of Milan where he achieved the Ph.D. in Mechanical Engineering in 2019. His research interest focuses on the development of vision based techniques applied to mechanical and thermal measurements, focusing on vibration and shock testing.

Ruben Balcaen just finished his Ph.D. on uncertainty quantification in stereo-DIC using a self programmed FE based image generator at the department of Materials Engineering of KU Leuven.

Emanuele Zappa - M'2010 received the Ph.D. degree in Applied Mechanics from Politecnico di Milano in 2002. From 2001 he works at the Dept. of Mechanical Engineering where he is now Associate Professor. He is author of several publications in the field of measurements, with focus on vision techniques.

Dimitri Debruyne is professor at the Department of Materials Engineering at KU Leuven. His research interests include optical strain measurement (especially DIC), material identification via inverse methods, FE modelling, metal forming and the forming and mechanical behaviour of joints (clinching, riveting, bolting and welding). He is the co-founder of two spinoffs (Indurium in 2008, MatchID in 2015).